AGU PUBLICATIONS

JGR

Journal of Geophysical Research: Space Physics

RESEARCH ARTICLE

10.1002/2014JA020274

Key Points:
- Mass density at L=11 is estimated from toroidal wave frequency
- Solar flux, represented by F10.7, controls the density
- The mass density varies by a factor of 2 over a solar cycle

Correspondence to:
K. Takahashi,
kazue.takahashi@jhuapl.edu

Citation:
Takahashi, K., R. E. Denton, M. Hirahara, K. Min, S. Ohtani, and E. Sanchez (2014), Solar cycle variation of plasma mass density in the outer magnetosphere: Magnetoseismic analysis of toroidal standing Alfvén waves detected by Geotail, *J. Geophys. Res. Space Physics*, *119*, 8338–8356, doi:10.1002/2014JA020274.

Received 16 JUN 2014
Accepted 23 SEP 2014
Accepted article online 26 SEP 2014
Published online 23 OCT 2014

Solar cycle variation of plasma mass density in the outer magnetosphere: Magnetoseismic analysis of toroidal standing Alfvén waves detected by Geotail

Kazue Takahashi[1], Richard E. Denton[2], Masafumi Hirahara[3], Kyungguk Min[4], Shin-ichi Ohtani[1], and Ennio Sanchez[5]

[1]Johns Hopkins University Applied Physics Laboratory, Laurel, Maryland, USA, [2]Department of Physics and Astronomy, Dartmouth College, Hanover, New Hampshire, USA, [3]Solar-Terrestrial Environment Laboratory, Nagoya University, Nagoya, Japan, [4]Department of Physics, Auburn University, Auburn, Alabama, USA, [5]Center for Geospace Studies, SRI International, Menlo Park, California, USA

Abstract We study the variation of plasma mass density in the outer magnetosphere over a solar cycle using mass density estimated from the frequency of fundamental toroidal standing Alfvén waves observed by the Geotail spacecraft. We identify wave events using ion bulk velocity data covering 1995–2006 and use events in the 0400–0800 magnetic local time sector for statistical analysis. We find that the $F_{10.7}$ index is a dominant controlling factor of the mass density. For the equatorial mass density ρ^*_{eq} that is normalized to the value at $L = 11$, we obtain an empirical formula $\log \rho^*_{eq} = -0.136 + 1.78 \times 10^{-3} F_{10.7}$, where the units of ρ^*_{eq} and $F_{10.7}$ are amu cm^{-3} and solar flux units (sfu; 1 sfu =10^{-22} W m^{-2} Hz^{-1}), respectively. This formula indicates that ρ^*_{eq} changes by a factor of 1.8, if $F_{10.7}$ changes from 70 sfu (solar minimum) to 210 sfu (solar maximum). A formula derived in a similar manner using GOES magnetometer data indicates that, for the same range of $F_{10.7}$, the mass density at $L \sim 7$ varies by a factor of 4.1 We attribute the smaller factor at $L = 11$ to the lower O^+/H^+ number density ratio at higher L, the stronger $F_{10.7}$ dependence of the O^+ outflow rate than the H^+ outflow rate, and entry of solar wind H^+ ions to the outer magnetosphere.

1. Introduction

Mass density, denoted ρ, is a fundamental quantity of the magnetospheric plasma that determines the velocity of magnetohydrodynamic (MHD) waves and thus the timescale of various large-scale phenomena. Despite this importance, the density is often poorly known, because particle experiments in general cover only a portion of the full multi-ion distribution function that is necessary to determine the mass density. This difficulty makes the indirect technique known as magnetoseismology an attractive alternative for gaining information on the mass density [*Chi and Russell*, 2005; *Denton*, 2006; *Menk and Waters*, 2013].

The magnetoseismology technique is based on the fact that MHD wave velocity depends on the mass density. Among MHD waves in the magnetosphere, the most often used in this technique are toroidal standing Alfvén waves, which are azimuthal eigenoscillations (or normal modes) of geomagnetic field lines. An approximate frequency of the nth harmonic, f_{Tn}, of the oscillations is given in terms of the Alfvén wave time-of-flight integral between the southern and northern footpoints of the magnetic field line as

$$f_{Tn} = n \left[\oint B^{-1} (\mu_0 \rho)^{1/2} \mathrm{d}s \right]^{-1}, \quad (1)$$

where B is the magnetic field magnitude and s is distance along the magnetic field line. Note that $n = 1$ corresponds to the fundamental mode.

The magnetoseismology technique has been widely used to investigate the magnetospheric mass density and ion composition. On the ground, toroidal wave frequencies determined with the magnetic field cross phase technique [*Waters et al.*, 1991] are used to estimate the mass density at various latitudes [*Vellante et al.*, 2007; *Menk and Waters*, 2013]. In space, toroidal waves cause oscillations in the electric field, magnetic field, and particle fluxes, and the frequencies of these oscillations have been used to estimate the mass density in the inner magnetosphere ($L < 7$) [*Takahashi et al.*, 2006], at geostationary orbit ($L \sim 7$) [*Takahashi et al.*, 2010], and in the outer magnetosphere ($L > 7$) [*Takahashi et al.*, 2002; *Min et al.*, 2013]. In some studies,

electron number density derived using various techniques is compared with mass density estimated from toroidal wave frequencies to infer the density of heavy ions, O^+ in particular [*Takahashi et al.*, 2006, 2008; *Grew et al.*, 2007; *Denton et al.*, 2011; *Nosé et al.*, 2011].

Recent studies reported that the solar extreme ultraviolet radiation, represented by the $F_{10.7}$ index given in the solar flux units (sfu) of 10^{-22} W m^{-2} Hz^{-1}, is a dominant controlling factor of the mass density and ion composition at geosynchronous orbit. According to *Takahashi et al.* [2010], the mass density was positively correlated with $F_{10.7}$ and varied by a factor of ~5 over a solar cycle, during which $F_{10.7}$ varied between 68 and 255 sfu. This variation was attributed to the increase of the O^+ density relative to the electron density, from $\sim 2 \times 10^{-3}$ at solar minimum to ~0.2 at solar maximum [*Denton et al.*, 2011]. Solar cycle variation of the mass density is poorly known beyond geosynchronous distance, although enhancement of O^+ flux at solar maximum has been reported at Geotail [*Hirahara et al.*, 2004]. This lack of information is the primary motivation for the present study.

In this paper we present a statistical study of the mass density in the outer magnetosphere ($L > 9$) using the frequency of toroidal waves observed by the Geotail spacecraft. We apply basically the same magnetoseismic technique used in previous satellite studies [*Takahashi et al.*, 2002; *Denton et al.*, 2011] to Geotail data to estimate the mass density. We examine the dependence of the estimated mass density on $F_{10.7}$, solar wind and interplanetary magnetic field (IMF) parameters, and geomagnetic activity. We find that the mass density evaluated at $L \sim 11$ in the dawn sector is positively correlated with $F_{10.7}$ similar to previous GOES satellite results at $L \sim 7$ [*Takahashi et al.*, 2010], but that the degree of the density variation over a solar cycle is smaller at $L \sim 11$.

The remainder of this paper is organized as follows. Section 2 describes the experiments and data, section 3 describes an example event, section 4 presents statistical analyses, section 5 presents discussion, and section 6 concludes the study.

2. Experiments and Data

The Geotail satellite was launched on 24 July 1992 to explore the magnetotail at geocentric distances up to 220 R_E. Since 1995, the spacecraft has been placed on orbits with perigee at ~9 R_E (geocentric), apogee at ~30 R_E, inclination of −7° with respect to the ecliptic plane, and an orbital period of ~5 days. We use data acquired from January 1995 to early March 2006, spanning solar cycles 22 and 23. During the selected time period, the perigee of the spacecraft was located at geocentric distances between 8.3 R_E and 10.5 R_E. Therefore, the perigee was often in the solar wind when the spacecraft was near noon, but it was mostly inside the magnetosphere at dawn and dusk.

Geotail data used in the present study have been acquired by the low-energy particle (LEP) experiment [*Mukai et al.*, 1994] and the magnetic field experiment [*Kokubun et al.*, 1994]. We use daily data files provided by the Japan Aerospace Exploration Agency that contain ion moments determined on board the spacecraft at the cadence of 4 spin periods (~12 s) and magnetic field (**B**) vectors averaged to the same cadence. The LEP experiment covers ion energy from 32 eV/e to 43 keV/e, and the ion moments include the three components of the bulk velocity **V**. We express the Geotail vector data in the local right-handed ν-ϕ-μ coordinate system, where $\mathbf{e}_\mu$ is parallel to the measured magnetic field vector, $\mathbf{e}_\phi$ (positive eastward) is in the direction of $\mathbf{e}_\mu \times \mathbf{R}_{SC}$ ($\mathbf{R}_{SC}$ is the spacecraft position vector relative to the center of the Earth), and the radial direction (positive outward) is given by $\mathbf{e}_\nu = \mathbf{e}_\phi \times \mathbf{e}_\mu$.

Because toroidal waves can be excited at multiple harmonics, it is necessary to correctly identify the harmonic mode to reliably estimate the mass density. To this end, we examine the **V** data instead of the **B** data, because the fundamental toroidal mode (referred to as T1 hereinafter) is usually the most powerful among the toroidal harmonics and the T1 mode is much easier to identify in **V** than **B**. We explain this using Figure 1, which illustrates the magnetic latitude (MLAT) dependence of the amplitude of the B_ϕ, V_ϕ, and E_ν components of a theoretical T1 wave excited at $L = 10$. The wave structures were obtained by numerically solving the toroidal wave equation of *Cummings et al.* [1969] for the mass density variation along the field line given by

$$\rho = \rho_{eq}(LR_E/R)^\alpha, \tag{2}$$

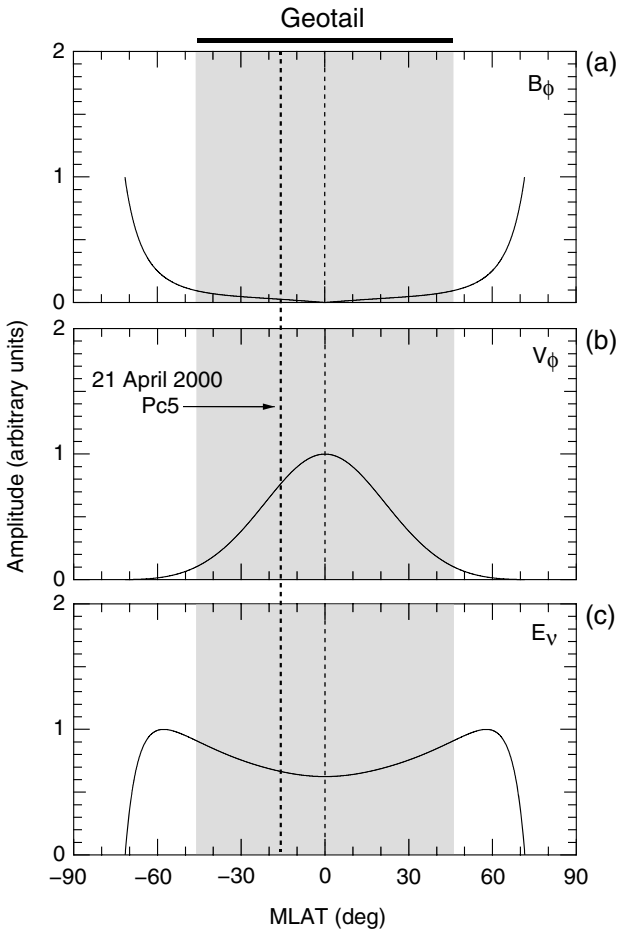

Figure 1. Numerical model of the amplitude of a fundamental toroidal wave on the dipole magnetic field line at L = 10, plotted as a function of MLAT. The shading indicates the MLAT range covered by Geotail. The heavy dashed line indicates the MLAT of the Pc5 wave event shown in Figure 2. (a) Azimuthal component of the magnetic field. (b) Azimuthal component of the plasma bulk velocity. (c) Radial component of the electric field.

where ρ_{eq} is the mass density at the magnetic equator, R is geocentric distance to the field line, and the exponent α is a free parameter that specifies the mass density variation along the field line. We adopted $\alpha = 1$ [e.g., *Denton et al.*, 2006] for Figure 1. In each panel, the shading indicates the range of MLAT covered by Geotail.

The field line mode structure varies among the three selected quantities. Figure 1a shows that the amplitude of B_ϕ is zero (node) at the equator and increases approximately linearly from there up to the Geotail MLAT limits of ±47°. This means that the detection rate of the T1 mode strongly depends on MLAT if we use **B**-field data. This is not the case with **V**. Figure 1b shows that the V_ϕ amplitude is peaked at the magnetic equator and is finite in the MLAT range of Geotail, making V_ϕ an ideal quantity for T1 event detection near the magnetic equator. The E_ν amplitude structure (Figure 1c) is also suited for T1 event detection at the Geotail position. Although Geotail measures the **E** field [*Tsuruda et al.*, 1994], we do not use the **E** field data because the field is measured only in the satellite spin plane and the measurements are sometimes affected by satellite wake, uneven illumination of the sensors by the sunlight, or spacecraft charging [*Hartinger et al.*, 2013].

3. Analysis of a Toroidal Wave Event

We describe the property of toroidal waves at Geotail using a Pc5 wave event on 21 April 2000. This event is very typical at Geotail and is chosen because *Hirahara et al.* [2004] reported detection of cold heavy ions with the LEP experiment during the same wave event. We will examine the ion data in section 5.1.

3.1. Wave Properties

Figure 2 shows an overview of the event. At 2130 universal time (UT), the center of the 3 h period shown, Geotail was located at (5.03, −6.66, −4.05 R_E) in the geocentric solar magnetospheric (GSM) coordinates, which corresponds to the dipole coordinates (L, MLAT, magnetic local time (MLT)) of (10.1, −16.2°, 8.8 h). The parameter labeled $n_{i\_onboard}$ in Figure 2a is the ion number density computed on board the spacecraft by taking the moment of the ion flux measured by the LEP instrument assuming that the ions are all protons. Under normal circumstances, the ions that contribute to the moment at the Geotail position for Figure 2 have plasma sheet energies (>1 keV). The same panel shows the electron number density n_e estimated from the cutoff at the plasma frequency of the continuum radiation observed by the Geotail plasma wave instrument [*Matsumoto et al.*, 1994]. We note that $n_{i\_onboard}$ can have a large error, because the ion counts may be contaminated by penetrating flux of energetic particles. For instance, the relationship $n_{i\_onboard} > n_e$ seen at 2150–2240 UT suggests that such contamination occurred.

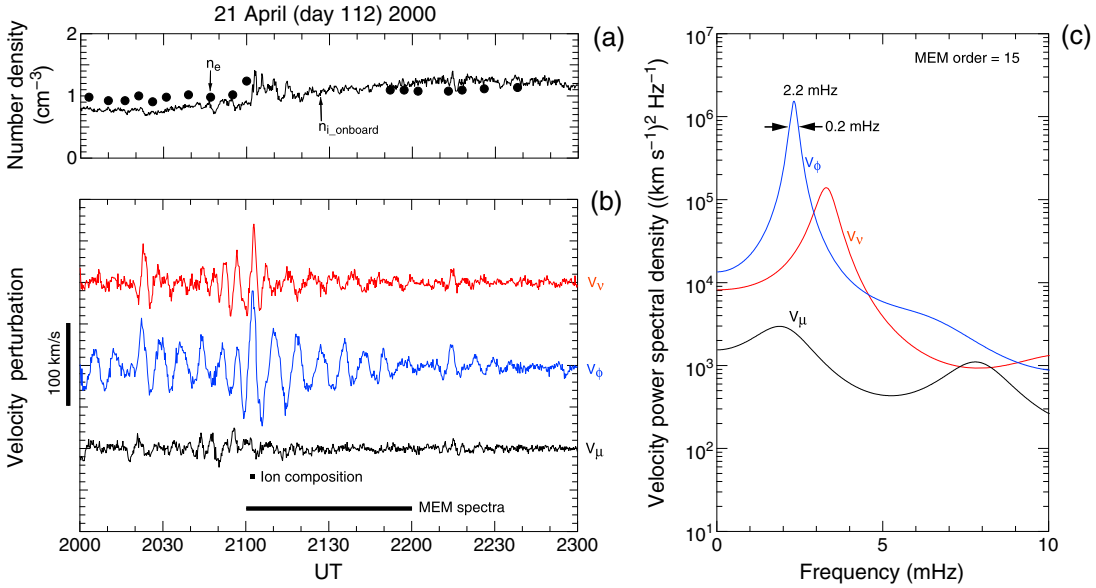

Figure 2. A Pc5 pulsation event at Geotail reported by *Hirahara et al.* [2004]. (a) Ion number density computed on board the spacecraft ($n_{i\_onboard}$, continuous line) and electron number density estimated from the cutoff at the plasma frequency of the continuum radiation (n_e, dots). (b) Time series of the three components of the ion bulk velocity. The short horizontal bar labeled "Ion composition" indicates a 90 s segment for which the density of cold H^+, He^+, and O^+ ions can be determined from measured ion fluxes. (c) The power spectral density of the velocity components computed for the 1 h segment marked by the black horizontal bar in Figure 2b.

In Figure 2b, V_ϕ exhibits continuous but amplitude-modulated oscillations with a period of ~500 s (Pc5 band). The V_ϕ amplitude suddenly increased at ~2100 UT in association with a large pulse in V_v and then steadily decreased for ~8 cycles until another small increase occurred at ~2210 UT, again in association with a small pulse in the V_v component.

Figure2c shows the power spectra computed from the **V** data for 2100–2200 UT using the maximum entropy method (MEM) [*Ulrich and Bishop*, 1975; *Press et al.*, 1986] with the MEM order of 15. A strong peak is seen in the V_ϕ spectrum at 2.2 mHz with a full width at half maximum (FWHM) of 0.2 mHz. Peaks occur in the V_v and V_μ spectra, but they are located at different frequencies with power much lower than that at the V_ϕ spectral peak.

Examination of magnetic field data provides evidence that the observed V_ϕ oscillations are associated with toroidal standing waves. Figure 3a is a schematic illustration of the relationship between **V** and **B** for a fundamental toroidal wave [e.g., *Singer and Kivelson*, 1979] (justification for considering only the fundamental mode is provided in section 3.2). This model predicts that, slightly south of the magnetic equator (green horizontal dashed line corresponding to the Geotail position), V_ϕ leads B_ϕ by a quarter of the wave period (Figure 3b). This is indeed what we observe. Figure 3c compares a 30 min segment of the measured V_ϕ and B_ϕ during the event shown in Figure 2. Note that for this plot, we defined the azimuthal component using a local mean field-aligned coordinate system in which the mean magnetic field direction is defined by 30 min running averages of the measured **B**. The black dashed line, which is the V_ϕ data shifted by +120 s (= quarter of the wave period), matches the phase of B_ϕ as predicted.

3.2. Mass Density Estimated With Megnetoseismic Technique

We used the wave equation derived by *Singer et al.* [1981] to relate the observed toroidal wave frequency to the mass density. To solve the equation, we need to select a magnetic field model and specify a functional form of the mass density variation along the magnetic field line. For the magnetic field we used the model by *Tsyganenko and Sitnov* [2005], referred to as TS05. At the Geotail position at 2130 UT, the model magnetic field is (25.5, −23.6, 44.9 nT) in GSM. The measured magnetic field averaged over the data window 2100–2200 UT for the MEM power spectra (Figure 2b) is (28.6, −24.5, 38.7 nT) in GSM. The model and observation differ only by 5% in magnitude (the model field is stronger) and 8° in direction. We consider the model to be realistic. For the mass density field line variation, we use the model given by equation (2) with

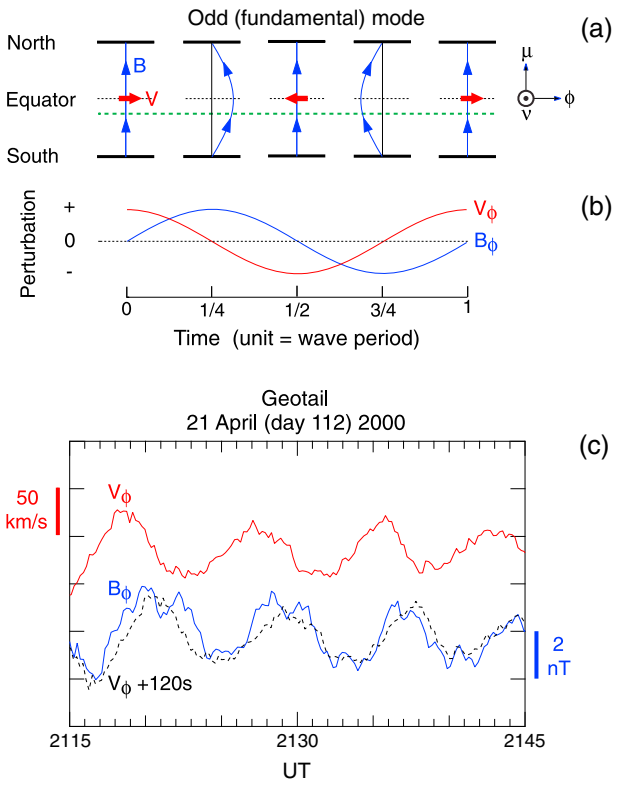

Figure 3. (a) Illustration of oscillations of the velocity **V** and magnetic field **B** during one cycle of a fundamental toroidal wave. The magnetic field is anchored to the ionosphere at the north and south ends, with the black horizontal dashed line indicating the magnetic equator. The green horizontal dashed line indicates the location of Geotail. (b) The temporal variation of the azimuthal component of **V** and **B** evaluated at the Geotail position shown in Figure 3a. (c) Measured velocity and magnetic field. The black dashed line indicates V_ϕ that is shifted to the right by 120 s (a quarter of the wave period).

$\alpha = 1$. The reason for this choice and how use of different α values affect the mass density estimates are described in section 5.1.

The numerical solution of the Singer et al. equation yields a mass density value $\rho = 3.1$ amu cm^{-3} at the Geotail position, if we assume the oscillations to be the fundamental mode. This mass density in turn gives an average ion mass value, M ($= \rho/n_e$), of ~3 amu, according to the n_e value of ~1 cm^{-3} shown in Figure 2a. In the Earth's magnetosphere, M should be somewhere between 1 amu (all-H^+ plasma) and 16 amu (all-O^+ plasma), and an M value greater than 1 amu means a finite amount of heavy ions. We note that the above event occurred near solar maximum, when the O^+ density is high at geosynchronous orbit [*Denton et al.*, 2011].

In estimating the mass density it is crucial that we correctly determine the harmonic mode of toroidal waves. Although toroidal waves are excited at multiple harmonics, it is highly unlikely that the narrowband V_ϕ oscillations at Geotail that we identify as T1 events originate from anything other than the fundamental toroidal mode. For example, consider the waves shown in Figure 3. The oscillations cannot be the second harmonic mode, because in that mode V_ϕ should lag behind B_ϕ by ~90°, opposite to what was observed. The oscillations cannot be the third harmonic, either. Although the third harmonic is consistent with the observed V_ϕ-B_ϕ phase delay, it gives an unrealistic mass density value. If we assume the 2.2 mHz oscillation at 2130 UT to be the third harmonic, the fundamental frequency would be ~0.5 mHz, according to the T1/T3 frequency ratio obtained in dipole calculation [*Cummings et al.*, 1969] or obtained statistically from observations at geostationary orbit [*Takahashi and Denton*, 2007]. For the estimated fundamental frequency, the Singer et al. equation gives a solution ρ ~50 amu cm^{-3} at the spacecraft. With the n_e value of ~1 cm^{-3}, we get M ~ 50 amu, which is highly unrealistic.

4. Statistical Analysis

This section describes statistical analyses of the mass density derived from the T1 frequency observed at Geotail.

4.1. Selection of Toroidal Wave Events

We have selected toroidal wave events from the 12 year Geotail data set described in section 2. An automated procedure was developed to consistently and efficiently identify wave events from this large data set. The specific steps are as follows:

1. Wave events are identified in a 60 min data window that was stepped forward by 30 min. The data window covers UT segments 0000–0100, 0030–0130, etc.; and the time tag of each event is given at the center of the data window, 0030, 0100 UT, etc.

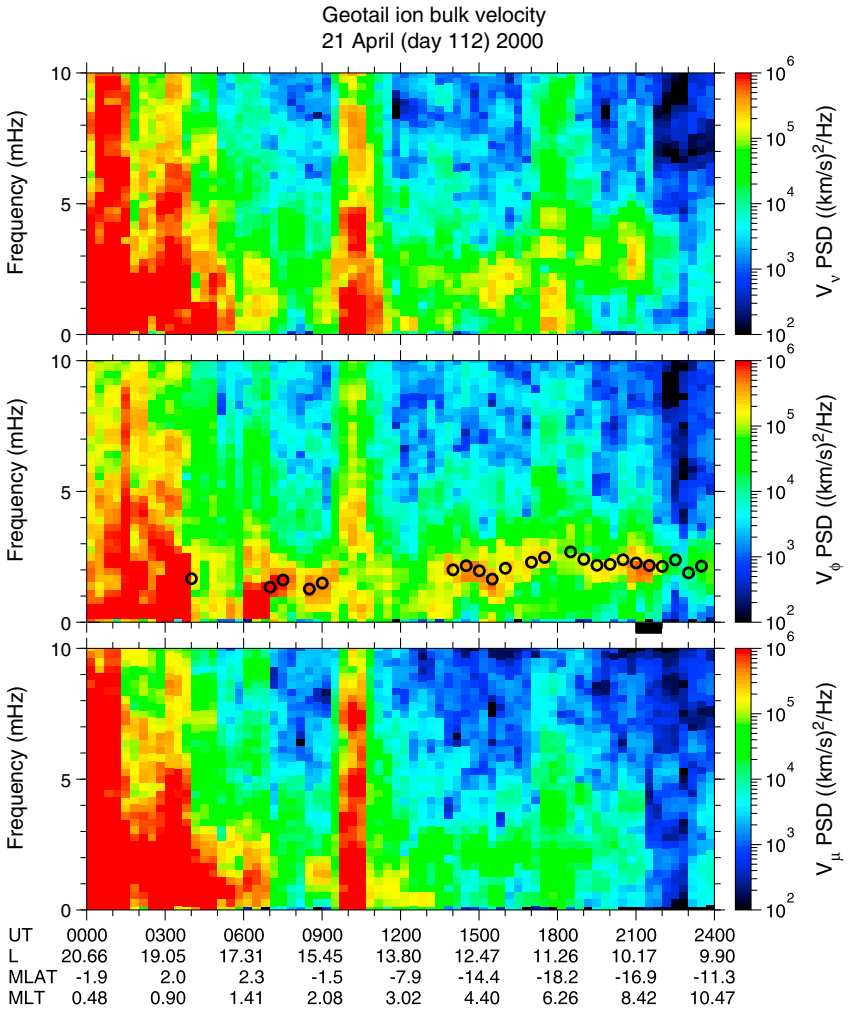

Figure 4. Dynamic spectra of the three components of the ion bulk velocity at Geotail for 21 April 2000. The spectra were obtained from the Fourier transform of data in a moving 60 min window. The spectra were smoothed by 3 point averaging. The open circles in the middle panel show the spectral peaks identified using MEM. The spacecraft position is shown at the bottom using the dipole-based coordinates: *L*, MLAT, and MLT.

2. If the ion bulk velocity has a tailward component exceeding 100 km/s, that is, $V_{xGSM} < -100$ km/s, the data segment is skipped, because the high velocity indicates that the spacecraft was in the solar wind or in the magnetosheath.
3. For the data segment that passed the V_{xGSM} test, the ion bulk velocity vector **V** is rotated into the magnetic field-aligned ν-ϕ-μ coordinates described in section 2.
4. The three components of the rotated **V** vector are subjected to MEM spectral analysis with a fixed MEM order of 15, as shown in Figure 2. The MEM order was chosen by comparison with spectra computed using Fourier transform and based on our experiences in previous magnetoseismology studies [e.g., *Takahashi et al.*, 2002]. Spectral peaks of the V_ϕ component are scanned, and the highest peak between 0 and the Nyquist frequency (~40 mHz) is selected as the possible indicator of a T1 wave. We evaluate the FWHM value for this peak and proceed to the next step if the bandwidth is smaller than 1.0 mHz. If not, we judge that no T1 wave was excited and skip the data segment.
5. If a narrowband spectral peak is identified in step 4, we integrate the power spectrum of the three components of **V** in the FWHM determined from the V_ϕ spectral peak. We reject the event if the integrated power of V_ϕ is smaller than that of V_ν or V_μ. A toroidal wave should have power strongest in V_ϕ.
6. We register the frequency, denoted f_{T1}, of the spectral peak of the toroidal wave that passed the above tests for the statistical analyses presented below.

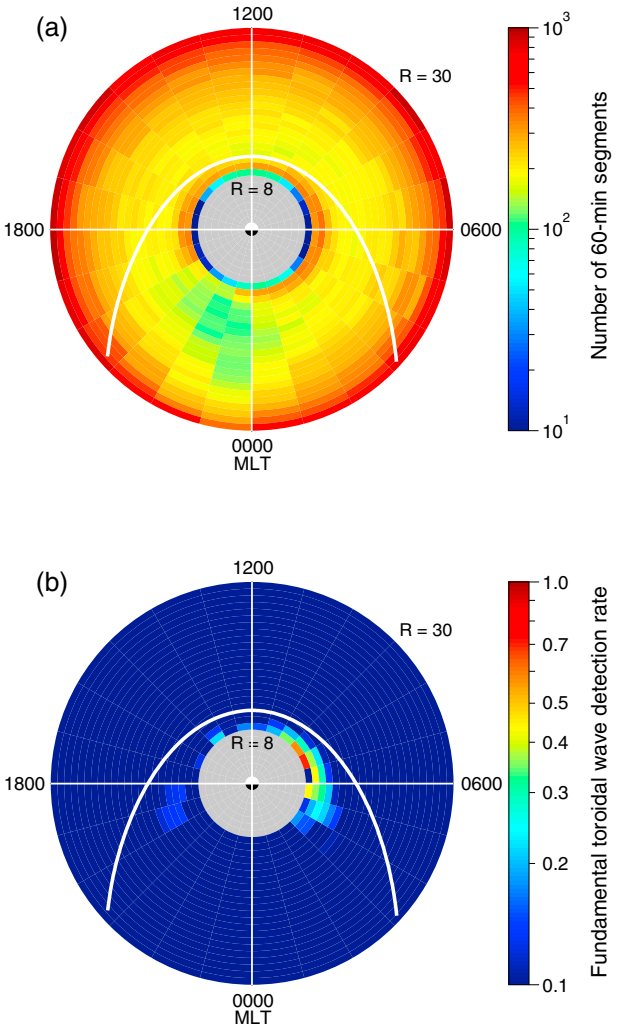

Figure 5. (a) Spatial coverage of Geotail data for 1995–2006 used in the statistical analysis. In this dial plot, the radius (R) is the radial distance, the azimuth is the MLT defined using a dipole magnetic field, and the color indicates the number of 60 min data segments. The bin size is 1 R_E for R and 1 h for MLT. (b) Rate of detection of fundamental toroidal waves.

Figure 4 illustrates the performance of our T1 event selection technique using dynamic spectra of the three velocity components generated using the Fourier transform method. In the 24 h spectra, narrowband V_ϕ oscillations between 1 and 3 mHz are evident from 0700 to 0900 UT and 1400 to 2300 UT. The open circles in the V_ϕ panel indicate the T1 spectral peaks determined with the MEM technique. The T1 event shown in Figure 2 (marked by a black bar at the bottom of the velocity panel) is part of this continuous wave activity. The good match between the MEM spectral peaks and the enhancement in the Fourier spectra confirms that our event identification technique works well in tracking prominent toroidal oscillations.

The velocity dynamic spectra usually exhibit a single outstanding spectral peak, unlike magnetic field dynamic spectra, which commonly contain multiple toroidal harmonics with comparable intensities [e.g., *Min et al.*, 2013]. The peak in the velocity spectra is usually the manifestation of the T1 mode as we described in section 3. With velocity data, there is no need for a human intervention in harmonic mode identification, which is a major task in performing statistical magnetoseismic analyses of magnetic field data [*Takahashi et al.*, 2010]. We also note that, for a given value of ρ_{eq}, the frequency of the T1 mode is less sensitive to the value of α than the frequency of higher harmonics [e.g., *Cummings et al.*, 1969]. Conversely, if we estimate ρ_{eq} from the T1 frequency, the estimate is less dependent on α. This gives a great advantage to the use of T1 frequencies in estimating ρ_{eq}.

4.2. Spatial Distribution of Toroidal Waves

The T1 event search was conducted on all Geotail data for 1995–2006 and resulted in 3142 samples (in units of 60 min intervals). Figure 5 shows the spatial map of the data coverage and the detection rate of T1 events. In these polar plots, the radius R is the geocentric distance in R_E and the azimuth is MLT defined using a centered dipole. The bin width is 1 R_E for R and 1 h for MLT. The white curve is the empirical magnetopause by *Fairfield* [1971]. Figure 5a shows the number of 60 min data segments for which both the magnetic field and ion bulk velocity data are available. The coverage is high near the perigee (~9 R_E) and apogee (~30 R_E) because the radial velocity of the spacecraft is zero at these locations. The data coverage is nearly uniform in MLT except for the low coverage in the evening sector.

The T1 detection rate (Figure 5b) is given by the number of the T1 events divided by the total number of 60 min segments in each R-MLT bin. The detection rate is high in the dawn sector but is very low in the dusk sector. This local time asymmetry of long-period ultra low frequency (ULF) waves at Geotail has already been reported by *Hirahara et al.* [2004] and *Kokubun* [2013]. Also, it is similar to the local time

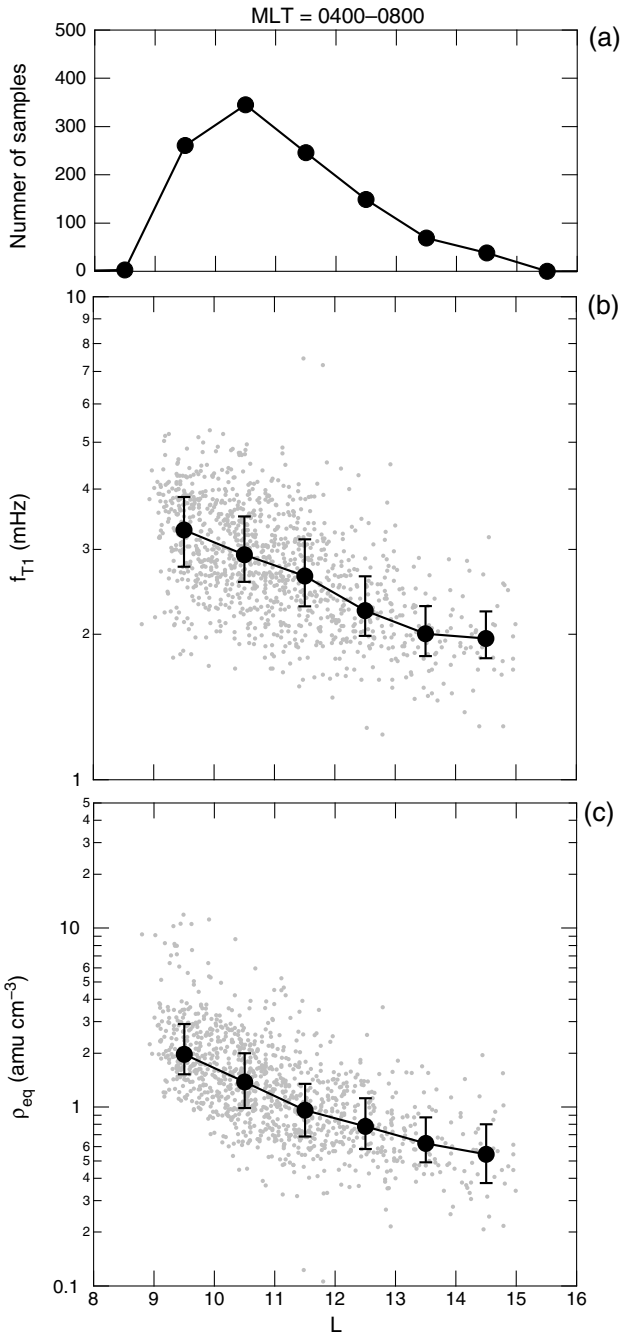

Figure 6. (a) *L* dependence of the number of T1 events in the 0400–0800 MLT sector. (b) *L* dependence of f_{T1}. The small gray dots are individual events. The heavy dots are medians computed in the *L* bins with the vertical bars indicating the range between the lower and upper quartiles. (c) Same as Figure 6b but for the equatorial mass density estimated from the f_{T1} data.

asymmetry reported on the ground [*Baker et al.*, 2003] and in the magnetosphere at $L < 10$ [*Anderson et al.*, 1990; *Nosé et al.*, 1995; *Takahashi et al.*, 2010; *Min et al.*, 2013].

Kokubun[2013] noted that statistically the IMF cone angle ($= \cos^{-1}(|B_x|/B)$) is lower when the ULF waves are observed at Geotail. This motivated us to examine the solar wind data for the Pc5 wave event shown in Figure 2. The time-shifted high-resolution OMNI data (http://omniweb.gsfc.nasa.gov/ow_min.html, now shown) indicate that there was no notable change in the solar wind velocity or density at ~2100 UT, when the toroidal wave intensified. However, the IMF cone angle rapidly increased from 28° at 2102 UT to 78° at 2104 UT, nearly simultaneous with the sudden enhancement of the amplitude of the toroidal wave that is seen in Figure 2b. This is contrary to the expectation from the statistical result reported by Kokubun and leads us to suggest that a transient plasma process occurring at the bow shock region produced a structure that impacted the magnetopause and excited toroidal waves [e.g., *Archer et al.*, 2013]. Across the IMF change at 2102–2014 UT, the IMF magnitude and the solar wind density varied little, so the change can be classified as a rotational discontinuity. A simulation study by *Lin et al.* [1996] showed that the interaction of a rotational discontinuity with the bow shock produces a strong pressure pulse in the magnetosheath. The pressure pulse propagates to the magnetopause and can trigger toroidal waves in a manner described by *Southwood and Kivelson* [1990]. Whether this mechanism explains the local time asymmetry of the T1 detection rate is a subject of future studies.

Of the 3142 T1 events that contributed to Figure 5b, 2397 events (76%) occurred in the region where the TS05 magnetic field model is closed. Because meaningful integration of the *Singer et al.* [1981] equation is possible only for closed field lines, we use this subset of T1 events in the following statistical analyses. We also use the TS05 model field to define magnetic coordinates of the spacecraft position: the magnetic equator is the location on the model field line that has the maximum geocentric distance, the *L* value is the geocentric distance to this equatorial point, and the MLT is the azimuth (about the dipole axis) of the equatorial point measured from the dipole midnight meridian.

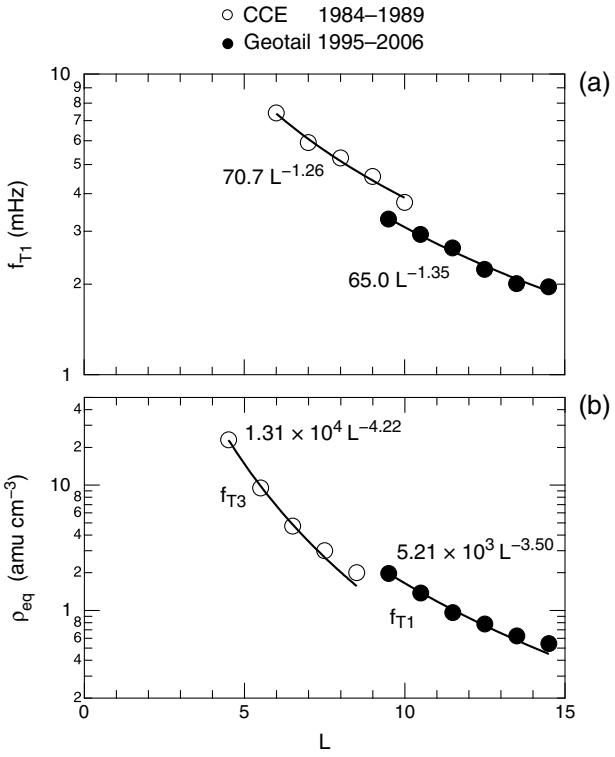

Figure 7. Comparison between studies of the radial distance dependence of toroidal wave frequency and estimated mass density. In each study, the magnetic field L shell is the maximum geocentric distance of a model field line that passes the spacecraft. (a) Median f_{T1} values at AMPTE/CCE in the 0400–0800 MLT sector [*Takahashi et al.*, 2002] (open circles) and the present Geotail result also for the 0400–0800 MLT sector (filled circles). (b) Median values of equatorial mass density estimated from toroidal wave frequencies in the dawn sector. The open circles indicate the results from the third harmonic frequency f_{T3} in the 0500–0700 MLT sector [*Min et al.*, 2013]. The filled circles indicate the present results for the 0400–0800 MLT sector.

4.3. L Dependence of f_{T1} and ρ_{eq}

Toroidal wave frequencies in general vary with L, so it is necessary to understand this variation before we evaluate the dependence of the frequencies and the derived mass density on other factors. Figure 6 shows the number of T1 events (Figure 6a), f_{T1} determined from the V_ϕ data (Figure 6b), and ρ_{eq} derived from f_{T1} (Figure 6c), all plotted as a function of L. In Figures 6b and 6c, the small dots indicate the individual samples, the heavy dots indicate the medians, and the vertical bars connect the lower and upper quartiles. The T1 events are distributed from $L = 9$ to 15, with a peak of 345 events in the 10–11 L bin. Although the data points exhibit considerable spread, it is clear that there is a general trend for both f_{T1} and ρ_{eq} to decrease with L. The f_{T1} values are mostly in the Pc5 band (1.6–6.7 mHz), in support of the common view that ground Pc5 pulsations originate from T1 waves in the outer magnetosphere.

Figure 7 repeats the L dependence of the median f_{T1} and ρ_{eq} values from Figure 6 and compares them with results from previous studies. Figure 7a includes the result from an Active Magnetospheric Particle Tracer Explorers (AMPTE)/CCE study [*Takahashi et al.*, 2002], which used energetic ion flux anisotropy oscillations to detect T1 events. For each set of data points, a power law function is fitted by the least squares method. For CCE, we obtain f_{T1} (mHz) = $70.7L^{-1.26}$, which is close to the Geotail result f_{T1} (mHz) = $65.0L^{-1.35}$. At L = 10–11, where the two studies overlap, the f_{T1} value is slightly higher for CCE. We attribute this offset to the $F_{10.7}$ dependence of mass density. The average $F_{10.7}$ was ~90 sfu for the period covered by the CCE study (1984–1989) and ~120 sfu for the period covered by the present Geotail study (1995–2006). Based on our GOES study [*Takahashi et al.*, 2010], we argue that the overall magnetospheric mass density was lower and the toroidal wave frequency higher during the CCE mission period, when $F_{10.7}$ was lower.

Figure 7b includes the result of another AMPTE/CCE study of mass density [*Min et al.*, 2013], which used multiharmonic toroidal waves identified in magnetometer data. Similar to Figure 7a, CCE and Geotail data points exhibit similar trends versus L, with a slight offset that can be explained by the same $F_{10.7}$ dependence. The Geotail portion of the data can be represented by $\rho_{eq}(\text{amu cm}^{-3}) = 5.21 \times 10^3\ L^{-3.50}$.

Noting that there is a strong L dependence of ρ_{eq} as shown in Figures 6 and 7, we normalize the mass density estimated at various L values to a common reference L value. This L normalization is a convenient technique in comparing the solar and solar wind dependence of mass density at GOES and Geotail. We assume that f_{T1} and ρ_{eq} at Geotail vary as $L^{-1.35}$ and $L^{-3.50}$, respectively, where the exponents are taken from the fitted functions shown in Figure 7. We have chosen $L = 11$ as the reference, because this is roughly the center of the L distribution of the detected T1 events (see Figure 6a). We use the asterisk to mark the L-normalized quantities: $f^*_{T1} = f_{T1}(L/11)^{1.35}$ and $\rho^*_{eq} = \rho_{eq}(L/11)^{3.50}$.

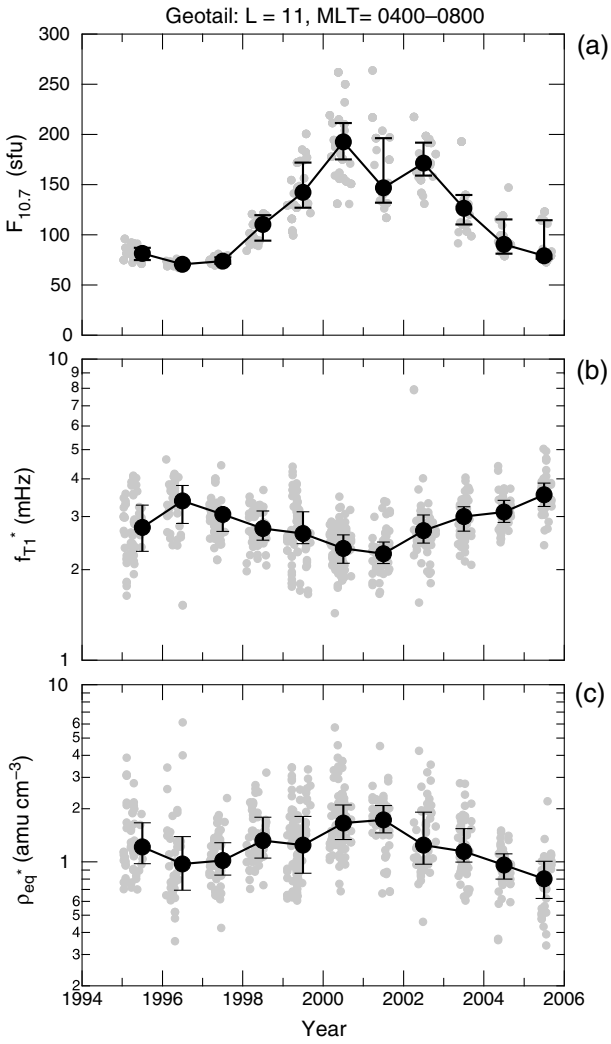

Figure 8. (a) Solar flux $F_{10.7}$ index at the time of the detected T1 events plotted as a function of time. The values of the index in yearly bins are used to define the median (filled circle) and the range between the lower and upper quartiles (vertical bars). (b) Same as Figure 8a except for the fundamental toroidal wave frequency normalized to $L = 11$ assuming an $L^{-1.35}$ dependence of the frequency. (c) Same as Figure 8b except for the density normalized to $L = 11$ assuming an $L^{-3.50}$ dependence of the density.

4.4. $F_{10.7}$ Dependence

$F_{10.7}$ is a known factor at geostationary orbit in controlling the toroidal wave frequency and mass density [*Takahashi et al.*, 2010; *Denton et al.*, 2011], so we first examine whether the same is true at Geotail. Figure 8 compares the time series of $F_{10.7}$, f_{T1}^*, and ρ_{eq}^* for 1995–2005. In each panel, the gray dots indicate individual data points, the heavy black dots are yearly medians, and the vertical bars connect the lower and upper quartiles. The individual data points are clustered in time, because Geotail passed the dawn sector only during a few-months period each year. Overall, we find an anticorrelation between $F_{10.7}$ and f_{T1}^* and a correlation between $F_{10.7}$ and ρ_{eq}^*. The median f_{T1}^* varies between 2.2 mHz at 2001 ($F_{10.7}$ = 147 sfu) and 3.54 mHz at 2005 ($F_{10.7}$ = 79 sfu). The median ρ_{eq}^* varies between 0.76 (at 2005) and 1.73 amu cm^{-3} (at 2001). Least squares fitting of a straight line to the relationship between the yearly median values of $F_{10.7}$ and the logarithm of ρ_{eq}^* (scatterplot shown in Figure 12) gives

$$\log \rho_{eq}^*(\text{amu cm}^{-3}) = -(0.136 \pm 0.060) + (1.78 \pm 0.48) \times 10^{-3} F_{10.7}(\text{sfu}), \quad (3)$$

where the numbers after the ± symbol are the standard deviations. The correlation coefficient between $\log \rho_{eq}^*$ and $F_{10.7}$ is 0.76.

The positive correlation between $F_{10.7}$ and the mass density is qualitatively in agreement with previous studies reporting satellite observations of the ion composition. At or near geostationary orbit (GEOS 1 and GEOS 2), *Young et al.* [1982] found that the density of O^+ ions in the 0.9–15.9 keV range rose dramatically by a factor of ~8 as $F_{10.7}$ increased from ~70 sfu to ~190 sfu. Such an increase was not observed for the H^+ and He^+ densities. Ion compositions observed from polar-orbiting DE-1 (0.01–17 keV/e) [*Yau et al.*, 1985] and Akebono (<1 eV to 70 eV/e) [*Cully et al.*, 2003] reported that the flux of upflowing ionospheric O^+ ions has a strong positive correlation with $F_{10.7}$. In the plasma sheet, the O^+ density computed from Geotail energetic ion data (9.4–212 keV/e) has a strong positive correlation with $F_{10.7}$ [*Nosé et al.*, 2009]. *Nosé et al.* [2009] estimated that the average ion mass (M) is ~1.1 amu at solar minimum and ~2.8 amu at solar maximum.

Because the above studies found that the dependence of the H^+ flux on $F_{10.7}$ is very weak compared with the O^+ flux, we attribute the mass density dependence on $F_{10.7}$ found in the present study to the dependence of O^+ flux on $F_{10.7}$. According to *Nosé et al.* [2009], the higher O^+ flux at times of higher $F_{10.7}$ (i.e., higher solar activity) occurs as the elevated solar ultraviolet (UV)/EUV intensity (for which $F_{10.7}$ is a good proxy) increases the O^+ density, temperature, and scale height in the ionospheric F layer. These UV/EUV effects are much weaker for H^+ ions.

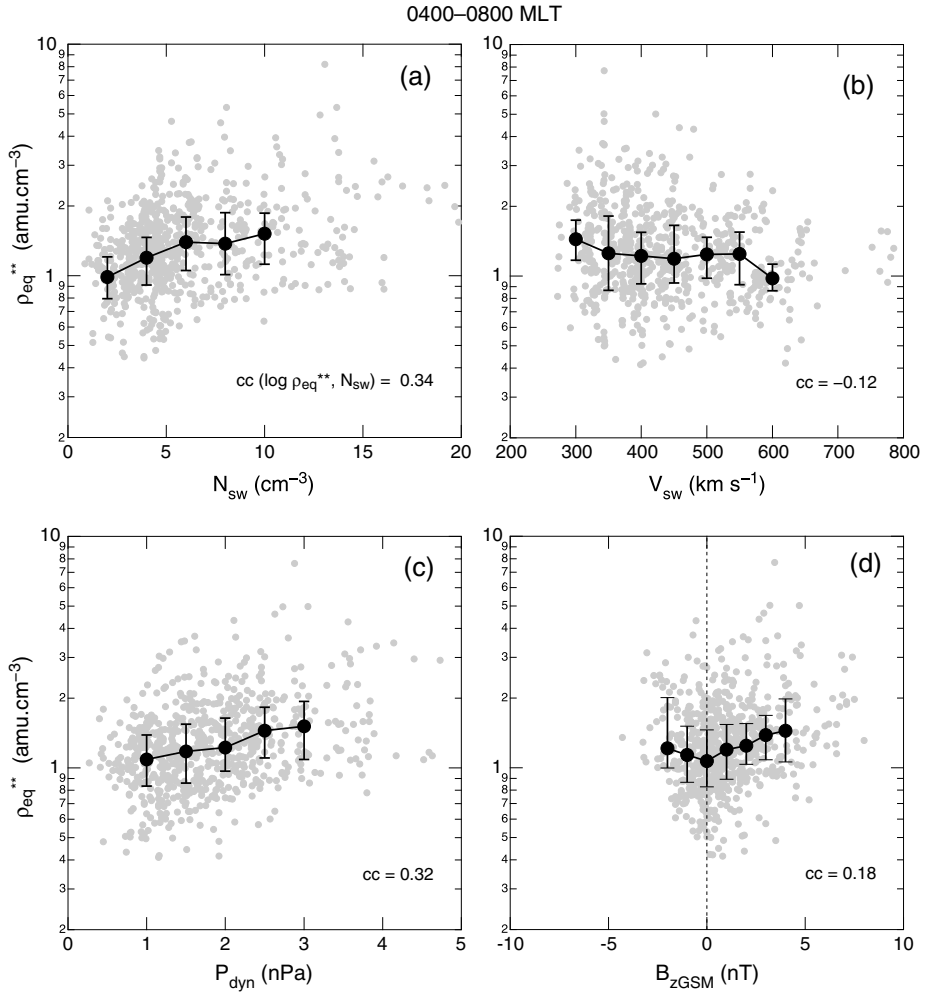

Figure 9. Dependence of ρ_{eq}^{**} (ρ_{eq} values normalized to L = 11 and $F_{10.7}$ = 124 sfu) on hourly solar wind parameters. The small dots are individual samples, the heavy dots are medians, and the vertical lines indicate the range between the lower and upper quartiles. The quartile values are shown only for bins with number of samples greater than 30. In each panel, the correlation coefficient (cc) between the logarithm of ρ_{eq}^{**} and the solar wind parameter is shown. (a) Dependence on the proton number density. (b) Dependence on the flow velocity. (c) Dependence on the dynamic pressure computed from the density and velocity. (d) Dependence on the GSM z component of the magnetic field.

4.5. Solar Wind Dependence

Solar wind dependence of the mass density is illustrated in Figure 9. We have chosen four solar wind parameters: number density N_{sw}, flow velocity V_{sw}, dynamic pressure P_{dyn} ($=N_{sw}M_i V_{sw}^2$, where M_i is the mass of ions including protons and alpha particles), and the GSM z component of the magnetic field B_{zGSM}. This choice is motivated by previous studies that examined the dependence of ion outflow from the ionosphere on various solar wind parameters. For example, in an Akebono study of ions with energy below 70 eV, *Cully et al.* [2003] found that the outflow rates of H^+ and O^+ are strongly correlated with solar wind dynamic pressure. In addition, they found that the outflow rates are correlated with solar wind density and anticorrelated with solar wind velocity.

In preparing Figure 9, we followed *Cully et al.* [2003] to correct the effects of $F_{10.7}$ on the mass density. Specifically, we used formula (3) to normalize individual ρ_{eq}^{*} value to the mean $F_{10.7}$ value of 124 sfu for 1995–2006. The corrected density is denoted ρ_{eq}^{**} and is given by

$$\rho_{eq}^{**} = 10^{1.78\times10^{-3}(124-F_{10.7})}\rho_{eq}^{*}. \quad (4)$$

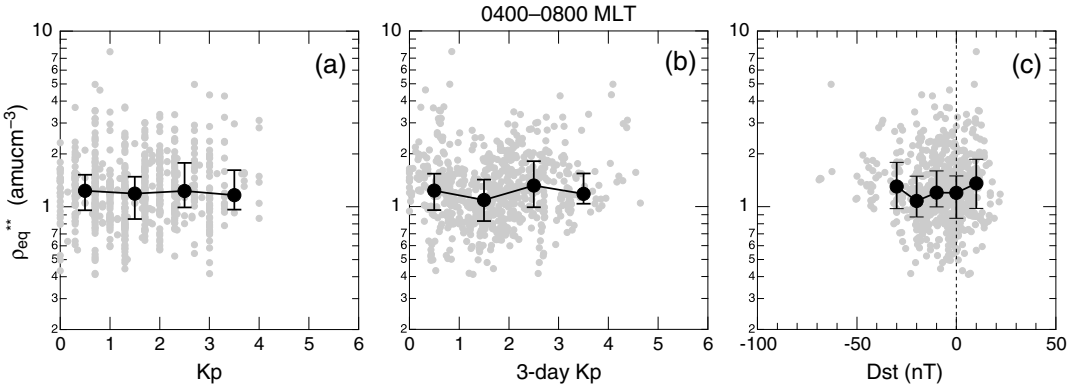

Figure 10. Dependence of ρ_{eq}^{**} on geomagnetic indices. The small dots are individual samples, the heavy dots are medians, and the vertical lines indicate the range between the lower and upper quartiles. The quartile values are shown only for bins with number of samples greater than 30. (a) Dependence on *Kp*. (b) Dependence on 3 day *Kp* defined in the text. (c) Dependence on *Dst*.

Although the ρ_{eq}^{**} data points are scattered considerably in each panel of Figure 9, we find some trends. First, ρ_{eq}^{**} has a positive correlation with N_{sw} (Figure 9a) and P_{dyn} (Figure 9c) but is uncorrelated with V_{sw} (Figure 9b). Because N_{sw} and P_{dyn} are interrelated by definition, it is not clear which of these is the physically meaningful controlling parameter of ρ_{eq}^{**}. The simplest explanation of the N_{sw}-ρ_{eq}^{**} correlation is that a fraction of the solar wind plasma enters the magnetosphere, possibly through the magnetopause Kelvin-Helmholtz instability [*Hasegawa et al.*, 2004].

The B_{zGSM}-ρ_{eq}^{**} relationship (Figure 9d) provides some insights into excitation of toroidal waves and entry of solar wind plasma into the magnetosphere. First, we find that the B_{zGSM} samples are distributed predominantly in the $B_{zGSM} > 0$ domain, from −2 to 5 nT. The lack of strongly negative B_{zGSM} samples means that few T1 events are detected when B_{zGSM} is strongly negative. We attribute this bias to magnetospheric disturbances (i.e., storms) that mask the occurrence of well-defined toroidal waves. Second, ρ_{eq}^{**} is positively correlated with B_{zGSM} within the $B_{zGSM} > 0$ domain. This could be the result of reconnection that allows entry of the solar wind plasma through the high-latitude magnetopause [*Song and Russell*, 1992; *Øieroset et al.*, 2008] or the result of diffusive entry of plasma at the low-latitude magnetopause through Kelvin-Helmholtz instability [*Miura*, 1984; *Otto and Fairfield*, 2000; *Nykyri and Otto*, 2001; *Hasegawa et al.*, 2009], which is more likely when the solar wind magnetic field is parallel to the magnetospheric magnetic field.

4.6. Geomagnetic Activity Dependence

Figure 10 illustrates the relationship between ρ_{eq}^{**} and geomagnetic activity indices. The indices chosen for analysis are *Kp*, 3 day *Kp* (Kp_{3d}), and *Dst*. The *Kp* and *Dst* indices are the original 3 h and 1 h values interpolated to the T1 epoch times, respectively. The 3 day *Kp* is the time average of the original *Kp*. For the current time t, the 3 day *Kp* is given by averaging over earlier times t' using the weighting factor $\exp[-(t - t')/t_0]$, where $t_0 = 3.0$ days [*Gallagher et al.*, 1988]. *Takahashi et al.* [2006] found that in the inner magnetosphere ($L < 7$) but mostly in the plasma trough, the mass density and the average ion mass (M) are correlated much better with Kp_{3d} than with the 3 h *Kp*.

In contrast to the results at $L \leq 7$, the mass density at Geotail shows very little dependence on *Kp* (Figure 10a) or Kp_{3d} (Figure 10b). The *Dst* index is not a strong controlling factor, either. However, we should note that the storm effects on the ion composition and mass density cannot be discussed in the present study, because our wave events occurred when *Dst* was higher than ∼−50 nT (Figure 10c).

5. Discussion

In this section we discuss (1) a comparison of mass densities obtained by direct and indirect methods, (2) solar cycle variations of the mass density at different distances, and (3) the relation of our results to previous particle studies.

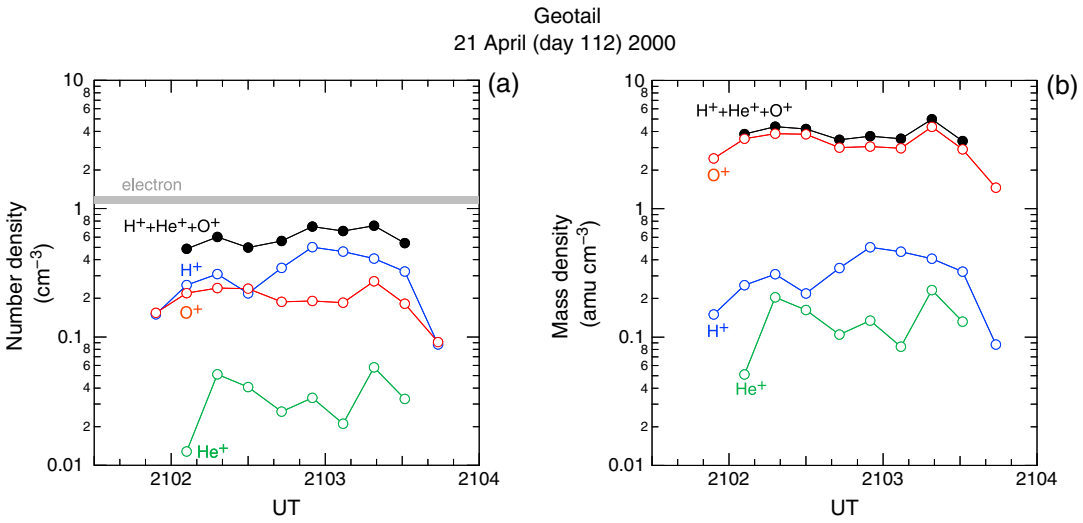

Figure 11. (a) Number densities of cold H^+ (blue), He^+ (green), and O^+ (red) ions along with the sum of these (black). The horizontal thick gray line indicates the range of electron number density (1.1–1.2 cm^{-3}) estimated before and after the ion measurements. (b) Partial and total mass densities corresponding to the ion number densities shown in Figure 11a.

5.1. Comparison of Mass Densities Derived by Direct and Indirect Methods

ULF waves add oscillatory bulk velocity to particles, and the elevated kinetic energy of low-energy (< 10 eV) particles may become higher than the lower-energy threshold of the particle detector. This phenomenon provides a unique opportunity for comparing mass densities estimated using magnetoseismic techniques with mass densities derived from measured particle fluxes. The Pc5 event shown in Figure 2 is one of the events reported by *Hirahara et al.* [2004] during which low-energy H^+, He^+, and O^+ ions were resolved as distinct populations in the LEP energy spectrum. The LEP experiment, which determines the particle energy per charge, does not distinguish ion species. However, when cold H^+, He^+, and O^+ ions are convected at the same bulk velocity, the kinetic energy carried by the three ions is mass dependent and the measured ion flux exhibits peaks at energies that have the ratio of 1:4:16. For example, the bulk velocity of 100 km/s translates to H^+, He^+, and O^+ kinetic energies of 53 eV, 210 eV, and 840 eV, respectively. The energies are all above the lower-energy threshold of LEP. As a result, the LEP energy spectra show peaks separated in energy by the expected ratio, and it is possible to manually take the moment of each population to obtain the number and mass densities for each species [*Hirahara et al.*, 2004]. *Lee and Angelopoulos* [2014] presented a more extensive study of the ion composition in the equatorial magnetosphere based on the same measurement principle. These authors used ion fluxes measured by the Time History of Events and Macroscale Interaction during Substorms (THEMIS) spacecraft and included flows associated with both ULF waves and magnetospheric convection.

Figure 11 illustrates the moments of the three ions during the toroidal wave event shown in Figure 2. The cold H^+, He^+, and O^+ populations were resolved over a ~90 s period when the Pc5 amplitude impulsively increased; and by taking the moments of the measured ion fluxes, we obtain the number density (Figure 11a) and the mass density (Figure 11b) of the three ion populations. Each data point in these figures corresponds to measurements made over four consecutive satellite spins (~12 s), and 8–10 consecutive density data points are obtained depending on the ions species. The H^+ number density is the highest overall. However, the O^+ number density is not much lower, and in fact it exceeds the H^+ density at one instance. This is in contrast to the O^+/H^+ typical number density ratio of 0.1–0.2 obtained from particle data [*Lennartsson and Shelley*, 1986; *Nosé et al.*, 2009; *Mouikis et al.*, 2010], although ratios near unity have been reported [*Maggiolo and Kistler*, 2014]. The sum of the number densities of the three ion species is 0.6 cm^{-3} when averaged over the eight duty cycles that cover all three ion species. In Figure 11b, we find that the O^+ ions make the largest contribution to the total mass density, accounting for ~90% of the total mass density. The total cold mass density averaged over the eight duty cycles is 3.9 amu cm^{-3}. This value is close to the value 3.1 amu cm^{-3} that is estimated from the fundamental toroidal wave frequency (see section 3.2).

Although the above result is encouraging, we need to remember that hot plasma sheet ions (energy > 1 keV) were also present and contribute to the mass density [see *Hirahara et al.*, 2004, Figure 2]. It is difficult to estimate the mass density of the hot ions because we do not know their composition. However, a rough estimate is possible. The electron number density surrounding the ion measurements are in the range 1.1–1.2 cm^{-3} (horizontal gray line in Figure 11a). By subtracting the cold ion density (0.6 cm^{-3}) described above from the electron density, we estimate that the number density of the hot ions is 0.5–0.6 cm^{-3}. If the ion composition of the hot plasma was dominated by H^+, then the mass density including both the hot and cold ions would be 4.5–4.6 amu cm^{-3}. However, it is more likely that the plasma sheet ions had an ion composition similar to that of the cold populations, in which case the total mass density would be 7.2–7.8 amu cm^{-3}. This latter value is 2.3–2.5 times the value 3.1 amu cm^{-3} that is estimated from the fundamental toroidal wave frequency.

We examine whether this mismatch can be explained by errors associated with the magnetoseismic analysis. First, there is an error in determining the wave frequency from wave signals that have finite duration and vary in amplitude and frequency. The Pc5 wave shown in Figure 2 had a frequency of 2.2 mHz and a bandwidth of 0.2 mHz, which translates to a $\sim \pm 10\%$ error in mass density according to equation (1). This error is much smaller than 2.5, so we consider the frequency error to be negligible. Second, there is the question on the assumptions that we made in relating the wave frequency to the mass density, including the background magnetic field (we used the TS05 model) and the mass density variation along the field line (we adopted $\alpha = 1$ in the mass density model, equation (2)). As for the magnetic field, the measured field at Geotail is close to the model as we described in section 3.2, so the model is considered to be satisfactory. On the other hand, the field line mass distribution has a large uncertainty. The model we adopted is based on our experience at $L < 7$ [*Takahashi et al.*, 2006; *Denton et al.*, 2006], but there is no guarantee that the same model works at $L > 9$.

We evaluate the α dependence of the estimated ρ_{eq}, using the toroidal wave equation for the dipole field by *Cummings et al.* [1969]. Use of a more realistic magnetic field (e.g., the TS05 model) is not essential here. To compare with the Geotail observation shown in Figure 2, we select a dipole field line at $L = 10$. For a fixed equatorial mass density of 1.0 amu cm^3, we find the f_{T1} values to be 3.82, 3.42, 3.34, and 2.71 mHz for $\alpha = -6, 0, 1$, and 6, respectively. The range $\alpha = 0$–6 is typically considered in the literature with $\alpha = 0$ representing a constant density along the field line and $\alpha = 6$ representing a rapid increase of the density along the field line from the equator to the ionospheric footpoints. The case $\alpha = -6$ is included here for an illustrative purpose, but it is not very realistic because it means a rapid decrease of the mass density from the magnetic equator toward the footpoints.

Because the toroidal wave frequency is inversely proportional to the square root of the mass density, we get the following ratios between the estimated mass densities for different values of α (for a fixed value of the observed fundamental toroidal frequency): $\rho_{eq}(\alpha = -6)/\rho_{eq}(\alpha = 1) = 1.31$, $\rho_{eq}(\alpha = 0)/\rho_{eq}(\alpha = 1) = 1.05$, and $\rho_{eq}(\alpha = 6)/\rho_{eq}(\alpha = 1) = 0.65$. Qualitatively, we can get higher ρ_{eq} values using larger negative values of α. However, even when we assume an unrealistic value of $\alpha = -6$, ρ_{eq} estimated from the toroidal wave frequency is raised only by a factor of 1.31 from 3.1 (for the case of $\alpha = 1$) to 4.1 amu cm^{-3} and falls short of what is estimated from the LEP data.

To conclude this subsection, although the mass density estimated from the toroidal wave frequency requires the presence of heavy ions (O^+ ions) in support of the particle measurements, the estimated mass density is lower than the total mass density of the cold and hot plasmas that is derived from the particle data. This discrepancy definitely needs to be addressed in future studies. However, we would like to emphasize that the mass densities derived through the magnetoseismic techniques are appropriate for correlative studies with solar wind and geomagnetic indices and for comparison between different regions (see section 5.3), as long as consistent methods are used in wave mode identification and in theoretically relating the observed frequencies to mass densities.

5.2. Comparison of GOES and Geotail Magnetoseismic Results

The present study is the first to address the solar cycle variation of the total plasma mass density in the outer magnetosphere ($L > 9$), so it is of great interest to compare the result with previous results at lower L. Figure 12 compares results from the present Geotail study and the GOES study by *Takahashi et al.* [2010]. In the GOES study, the frequency of the third harmonic toroidal waves, f_{T3}, was identified using magnetic field data from multiple satellites operated between 1980 and 1992. In Figure 12a, the yearly median

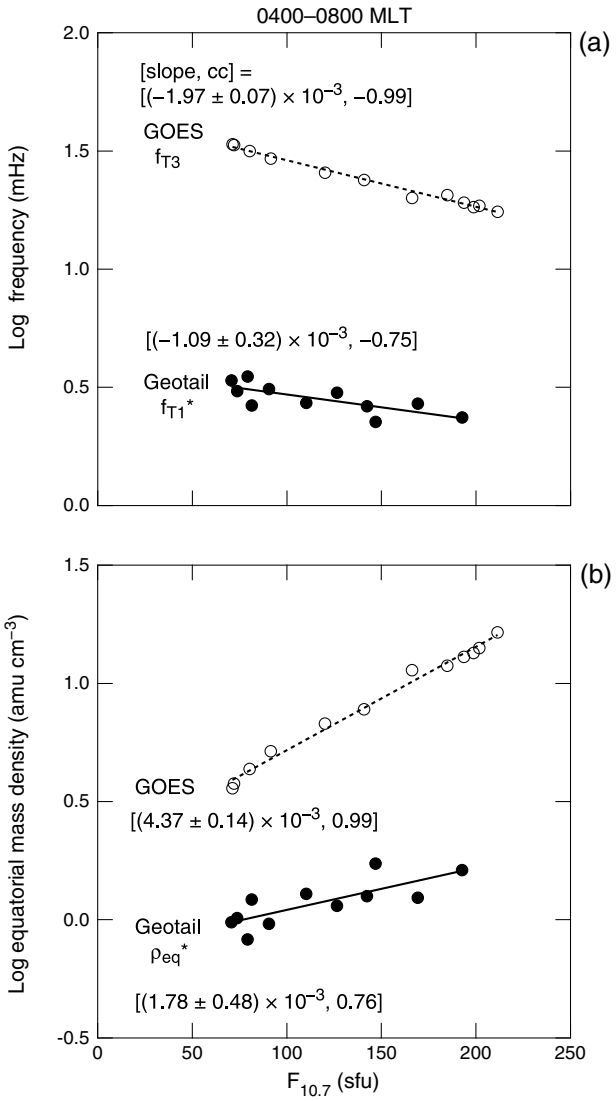

Figure 12. Comparison of results from GOES and Geotail studies. The scatterplots show yearly medians in the 0400–0800 MLT sector. The least squares method is used to fit a straight line to the data points. The values of the slope of the fitted line and its standard deviation are shown along with the value of the correlation coefficient (cc). (a) Toroidal wave frequency versus $F_{10.7}$. The frequency is for the third harmonic for GOES and the fundamental mode for Geotail. (b) Mass density versus $F_{10.7}$.

values of f_{T3} in the 0400–0800 MLT sector (open circles) are plotted versus the yearly median values of $F_{10.7}$. We find that f_{T3} is negatively correlated with $F_{10.7}$, which is well represented by the straight line $\log f_{T3}(\text{mHz}) = (1.66\pm0.01)-(1.97\pm0.07)\times10^{-3}F_{10.7}(\text{sfu})$, where the numbers after the ± symbols are standard deviations. The correlation coefficient (cc) between $\log f_{T3}$ and $F_{10.7}$ is −0.99. The median f_{T1}^* at Geotail (repeated from Figure 8b and shown by solid circles) is also negatively correlated with the median $F_{10.7}$ (repeated from Figure 8a). However, the frequency at Geotail has a weaker dependence on $F_{10.7}$, with the regression line given by $\log f_{T1}^*(\text{mHz}) = (0.578\pm0.039) - (1.09\pm0.32) \times 10^{-3}F_{10.7}(\text{sfu})$ and a correlation coefficient of −0.75.

Figure 12b shows the $F_{10.7}$ dependence of the mass density derived from the toroidal wave frequencies at Geotail and GOES. Because the mass density is proportional to the inverse of frequency squared (equation (1)), the density is positively correlated with $F_{10.7}$. The relationship between $F_{10.7}$ and the mass density at Geotail at $L \sim 11$ was already given by formula (3). At GOES, the relationship is given by

$$\log \rho_{eq}(\text{amu cm}^{-3}) = (0.280\pm0.022) + (4.37\pm0.14) \times 10^{-3}F_{10.7}(\text{sfu}). \quad (5)$$

The correlation coefficient between $\log \rho_{eq}$ and $F_{10.7}$ is 0.99.

These empirical formulas give different $F_{10.7}$ dependencies at Geotail and GOES. Formula (3) (Geotail) indicates that in the outer magnetosphere ($L \sim 11$), the mass density changes by a factor of 1.8, from 0.97 to 1.73 amu cm^{-3}, if $F_{10.7}$ changes by a factor of 3 from 70 sfu (solar minimum) to 210 sfu (solar maximum). Formula (5) (GOES) indicates that for the same range of $F_{10.7}$, the mass density at $L \sim 7$ varies a by factor of 4.1, from 3.9 to 16 amu cm^{-3}.

We pay attention to a few known facts about magnetospheric ions in interpreting the dependence of the mass density on the solar activity and position of observation. They are as follows.

1. O^+ ions originate only from the ionosphere, whereas H^+ ions originate from both the solar wind and the ionosphere.
2. The ionospheric O^+ production rate strongly depends on $F_{10.7}$, but the H^+ production rate does not [e.g., *Cully et al.*, 2003]. This means that, if both O^+ and H^+ ions are of ionospheric origin, the O^+/H^+ number density ratio determines how strongly the mass density depends on $F_{10.7}$. The dependence is stronger for

higher ratio. To explain the different slopes of the $F_{10.7}$-ρ relationship at GOES and Geotail (Figure 12b), the O^+/H^+ number density ratio is required to be higher at lower L. Note that depending on how the ionospheric ions are accelerated and transported, various O^+/H^+ number density ratios are possible in the equatorial magnetosphere.

3. The solar wind H^+ density does not depend on $F_{10.7}$ [*Feldman et al.*, 1978].
4. Transport of ionospheric O^+ ions to the magnetosphere does not occur uniformly in latitude. Three O^+ source regions have been discussed in the literature based on particle observations from polar-orbiting spacecraft: around the latitude of the plasmapause [*Chappell*, 1982],nightside auroral zone [*Yau and André*, 1997],and the cleft ion fountain [*Lockwood et al.*, 1985].

In the next section, we review previous studies on magnetospheric H^+ and O^+ ions and their implication for our magnetoseismic results.

5.3. Comparison With Ion Composition Studies Using Particle Experiments

Near the plasmapause, the Retarding Ion Mass Spectrometer instrument on the DE-1 satellite [*Chappell et al.*, 1981] detected O^+ ions at the thermal energy (<50 eV) that form a torus (oxygen torus) at L = 3–5 [*Horwitz et al.*, 1984; *Roberts et al.*, 1987; *Comfort et al.*, 1988]. The detection rate of the oxygen torus does not depend on geomagnetic activity level [*Roberts et al.*, 1987], but the torus may become more prominent during the storm recovery phase [*Nosé et al.*, 2011]. The oxygen torus can be a major contributor to the mass density observed at geostationary orbit. When geomagnetic activity is low, the plasmapause can expand to the geostationary orbit, and it is plausible that the oxygen torus also moves to the geostationary orbit. However, it is unlikely that the torus extends much beyond L = 7, if the torus is limited to a region close to the plasmapause as reported in studies using DE-1 [e.g., *Horwitz et al.*, 1984] and Combined Release and Radiation Effects Satellite [*Nosé et al.*, 2011]. This localized O^+ source will contribute to the mass density at GOES but not at Geotail, which provides a qualitative explanation to the results summarized in Figure 12.

Ions with thermal energy higher than the cold (below ~1 eV) plasmaspheric ions but lower than the hot (above ~1 keV) plasma sheet ions are found to form a warm plasma cloak outside the plasmapause [*Chappell et al.*, 2008]. The cloak is at lower L at dawn and spreads to larger L as it wraps around toward the early afternoon. *Chappell et al.* [2008] showed by particle tracing calculation that the cloak is formed by ions that flow out of the polar cap ionosphere, cross the tail neutral plane at relatively small distances, and drift sunward through the dawnside magnetosphere. The cloak configuration proposed by *Chappell et al.* [2008, Figure 3] indicates that, in the dawn sector, geosynchronous orbit is inside the cloak but the Geotail perigee L~9 is near the outer edge of the cloak. The cloak ion population was reported by *Lee and Angelopoulos* [2014] in a study using the THEMIS spacecraft. At dawn, THEMIS detected O^+ ions in the cloak energy range at radial distances 8–12 R_E. In this distance range, the O^+ density is higher at smaller distance (their Figure 8a) as the cloak model predicts, but the O^+/H^+ number density ratio does not exhibit a clear L dependence (their Figure 8c). Therefore, the relevance of the cloak to our results shown in Figure 12 remains unclear.

Measurements of ion composition in the nightside plasma sheet indicate that the O^+/H^+ number density ratio is higher at smaller distances. The ion composition in the plasma sheet has been statistically studied using the Energetic Particle and Ion Composition (EPIC) experiment on Geotail, which measures energetic ions in the 9–210 keV energy range [*Williams et al.*, 1994]. *Nosé et al.* [2009] and *Ohtani et al.* [2011] reported that the O^+/H^+ number density ratio determined with EPIC strongly depends on the solar activity, with a higher ratio appearing when the solar activity is higher. In addition, *Ohtani et al.* [2011] noted that the O^+/H^+ number density ratio is higher at smaller distances to the Earth, which is qualitatively consistent with our results shown in Figure 12. A similar earthward gradient of the O^+/H^+ number density ratio was reported by *Mouikis et al.* [2010], who studied plasma sheet ion composition at 15–19 R_E with the Cluster Ion Spectrometry/COmposition and DIstribution Function analyzer(CIS/CODIF) [*Rème et al.*, 1997]. *Ohtani et al.* [2011] suggested that a significant portion of the O^+ ions is transported directly from the auroral zone ionosphere to the near-Earth region without being transported to the distant tail and then convected back to the near-Earth region. This scenario is supported by a statistical study of ions in the plasma sheet energy (1–40 keV) [*Maggiolo and Kistler*, 2014] with Cluster CIS/CODIF. This most recent study covered all local times outside the radial distance of 7 R_E and found that the O^+/H^+ density ratio is higher at smaller radial distances in the distance range between 7 and 10 R_E, including the dawn sector. This result is consistent with the result of our magnetoseismic analysis summarized in Figure 12.

Finally, we note the possible influence of solar wind plasma on the mass density estimated at Geotail. It is known that cold dense plasma of the solar wind origin enters the magnetosphere during the periods of northward IMF [*Lennartsson and Shelley*, 1986]. The cold plasma has been reported at geostationary orbit [*Thomsen et al.*, 2003], but its density increases toward the flanks of the magnetosphere [*Terasawa et al.*, 1997; *Wang et al.*, 2006]. Because the majority of our toroidal wave events were observed at times of northward IMF (Figure 9d), it is possible that the solar wind plasma contributed to the mass density, making the $F_{10.7}$ dependence of the mass density at Geotail weaker than that at GOES.

To summarize, we can explain the different $F_{10.7}$-ρ relationship between GOES and Geotail (Figure 12) by combining the following three aspects of the behavior of O^+ and H^+ ions. First, as demonstrated by measurements of the ion composition with various spacecraft, the ionospheric supply (outflow) of O^+ ions to the magnetosphere is higher at $L \sim 7$ than at $L > 9$. Second, H^+ ions of solar wind origin can enter the outer magnetosphere. Third, the density of H^+ ions (originating from either the solar wind or the ionosphere) does not depend on $F_{10.7}$ as strongly as the density of O^+ ions.

6. Summary and Conclusions

In summary, we have presented a magnetoseismic study of plasma mass density using the frequency of fundamental toroidal (T1) waves detected by Geotail. The spacecraft routinely detected T1 waves in the dawn sector of the outer magnetosphere ($L > 9$), and wave events occurring in this sector over a solar cycle were used to determine the controlling parameters of the mass density. As expected from previous observations at $L \leq 7$, we find $F_{10.7}$ to be a dominant factor in controlling the mass density. At $L \sim 11$, the $F_{10.7}$ dependence is expressed as $\log\rho_{eq}$ (amu cm^{-3}) $= -0.136 + 1.78 \times 10^{-3}\ F_{10.7}$ (sfu). This formula predicts a factor of 1.8 mass density variation over a typical solar cycle.

We noted that the degree of the solar cycle variation of mass density is smaller at Geotail ($L \sim 11$) than at GOES ($L \sim 7$). At GOES, the mass density varies by a factor of 4.1 over a typical solar cycle, according to the empirical formula between the mass density and $F_{10.7}$ derived from the magnetoseismic analysis using the third harmonic of toroidal waves. From a comparison of the magnetoseismic results with previous particle measurements, we suggested that higher O^+/H^+ density ratio at lower L is the cause of the difference between the Geotail and GOES results.

We revisited a Pc5 toroidal wave event reported by *Hirahara et al.* [2004] and compared the mass density derived from our magnetoseismic analysis with the mass density derived from measured ion fluxes and the electron number density estimated from the properties of plasma wave spectra. Mass density values from both methods, when compared with the electron number density, indicate that O^+ ions significantly contributed to the mass density. However, there was a large discrepancy in the mass density values from the two methods that needs to be addressed in future studies.

Acknowledgments

Work at the Johns Hopkins University Applied Physics Laboratory was supported by NSF grants ATM-0855924 and AGS-1106427 and NASA grant NNX13AE02G. Work at Dartmouth College was supported by NSF grant AGS-1105790 and NASA grant NNX10AQ60G. Daniel Kang assisted K.T. in processing Geotail data through the NASA/APL summer internship program. The authors are grateful to H. Kojima for providing the electron number density data shown in Figure 2. The *Kp* and $F_{10.7}$ indexes were obtained from NOAA at http://www.ngdc.noaa.gov/stp. The solar wind/IMF data were obtained from the GSFC/SPDF OMNIweb interface at http://omniweb.gsfc.nasa.gov. The Geotail data were obtained from JAXA at http://darts.isas.jaxa.jp/stp/geotail.

Larry Kepko thanks Massimo Vellante and Peter Chi for their assistance in evaluating this paper.

References

Anderson, B. J., M. J. Engebretson, S. P. Rounds, L. J. Zanetti, and T. A. Potemra (1990), A statistical study of Pc3–5 pulsations observed by the AMPTE/CCE magnetic field experiment, 1. Occurrence distributions, *J. Geophys. Res.*, *95*(A7), 10,495–10,523.

Archer, M. O., T. S. Horbury, J. P. Eastwood, J. M. Weygand, and T. K. Yeoman (2013), Magnetospheric response to magnetosheath pressure pulses: A low pass filter effect, *J. Geophys. Res. Space Physics*, *118*, 5454–5466, doi:10.1002/jgra.50519.

Baker, G., E. F. Donovan, and B. J. Jackel (2003), A comprehensive survey of auroral latitude Pc5 pulsation characteristics, *J. Geophys. Res.*, *108*(A10), 1384, doi:10.1029/2002JA009801.

Chappell, C. R. (1982), Initial observations of thermal plasma composition and energetics from Dynamics Explorer-1, *Geophys. Res. Lett.*, *9*, 929–932.

Chappell, C. R., S. A. Fields, C. R. Baugher, J. H. Hoffman, W. B. Hanson, W. W. Wright, H. D. Hammack, G. R. Carignan, and A. F. Nagy (1981), The retarding ion mass spectrometer on Dynamics Explorer-A, *Space Sci. Inst.*, *5*, 477–491.

Chappell, C. R., M. M. Huddleston, T. E. Moore, B. L. Giles, and D. C. Delcourt (2008), Observations of the warm plasma cloak and an explanation of its formation in the magnetosphere, *J. Geophys. Res.*, *113*, A09206, doi:10.1029/2007JA012945.

Chi, P. J., and C. T. Russell (2005), Travel-time magnetoseismology: Magnetospheric sounding by timing the tremor in space, *Geophys. Res. Lett.*, *32*, L18108, doi:10.1029/2005GL023441.

Comfort, R. H., I. T. Newberry, and C. R. Chappell (1988), Preliminary statistical survey of plasmaspheric ion properties from observations by DE 1/RIMS, in *Modeling Magnetospheric Plasma, Geophys. Monogr. Ser.*, vol. 44, edited by T. E. Moore and J. H. Waite Jr., pp. 107–114, AGU, Washington, D. C.

Cully, C. M., E. F. Donovan, A. W. Yau, and G. G. Arkos (2003), Akebono/Suprathermal Mass Spectrometer observations of low-energy ion outflow: Dependence on magnetic activity and solar wind conditions, *J. Geophys. Res.*, *108*(A2), 1093, doi:10.1029/2002JA009457.

Cummings, W. D., R. J. O'Sullivan, and P. J. Coleman Jr. (1969), Standing Alfvén waves in the magnetosphere, *J. Geophys. Res.*, *74*(3), 778–793.

Denton, R. E. (2006), Magneto-seismology using spacecraft observations, in *Magnetospheric ULF Waves: Synthesis and New Directions, Geophys. Monogr. Ser.*, vol. 169, edited by K. Takahashi et al., pp. 307–317, AGU, Washington, D. C.

Denton, R. E., K. Takahashi, I. A. Galkin, P. A. Nsumei, X. Huang, B. W. Reinisch, R. R. Anderson, M. K. Sleeper, and W. J. Hughes (2006), Distribution of density along magnetospheric field lines, *J. Geophys. Res.*, *111*, A04213, doi:10.1029/2005JA011414.

Denton, R. E., M. F. Thomsen, K. Takahashi, R. R. Anderson, and H. J. Singer (2011), Solar cycle dependence of bulk ion composition at geosynchronous orbit, *J. Geophys. Res.*, *116*, A03212, doi:10.1029/2010JA016027.

Fairfield, D. H. (1971), Average and unusual locations for the Earth's magnetopause and bow shock, *J. Geophys. Res.*, *76*, 6700–6716.

Feldman, W. C., J. R. Asbridge, S. J. Bame, and J. T. Gosling (1978), Long-term variations of selected solar wind properties: Imp 6, 7, and 8 results, *J. Geophys. Res.*, *83*(A5), 2177–2189, doi:10.1029/JA083iA05p02177.

Gallagher, D. L., P. D. Craven, and R. H. Comfort (1988), An empirical model of the Earths plasmasphere, *Adv. Space Res.*, *8*(8), 15–24.

Grew, R. S., F. W. Menk, M. A. Clilverd, and B. R. Sandel (2007), Mass and electron densities in the inner magnetosphere during a prolonged disturbed interval, *Geophys. Res. Lett.*, *34*, L02108, doi:10.1029/2006GL028254.

Hartinger, M. D., M. B. Moldwin, K. Takahashi, J. W. Bonnell, and V. Angelopoulos (2013), Survey of the ULF wave Poynting vector near the Earth's magnetic equatorial plane, *J. Geophys. Res. Space Physics*, *118*, 6212–6227, doi:10.1002/jgra.50591.

Hasegawa, H., M. Fujimoto, T.-D. Phan, H. Rème, A. Balogh, M. W. Dunlop, C. Hashimoto, and R. TanDokoro (2004), Transport of solar wind into Earth's magnetosphere through rolled-up Kelvin-Helmholtz vortices, *Nature*, *430*(7001), 755–758, doi:10.1038/nature02799.

Hasegawa, H., et al. (2009), Kelvin-Helmholtz waves at the Earths magnetopause: Multiscale development and associated reconnection, *J. Geophys. Res.*, *114*, A12207, doi:10.1029/2009JA014042.

Hirahara, M., K. Seki, Y. Saito, and T. Mukai (2004), Periodic emergence of multicomposition cold ions modulated by geomagnetic field line oscillations in the near-Earth magnetosphere, *J. Geophys. Res.*, *109*, A03211, doi:10.1029/2003JA010141.

Horwitz, J. L., R. H. Comfort, and C. R. Chappell (1984), Thermal ion measurements of the formation of the new outer plasmasphere and double plasmapause during storm recovery phase, *Geophys. Res. Lett.*, *11*(8), 701–704.

Kokubun, S. (2013), ULF waves in the outer magnetosphere: Geotail observation, 1 transverse waves, *Earth Planets Space*, *65*, 41–433.

Kokubun, S., T. Yamamoto, M. H. Acua, H. Hayashi, K. Shiokawa, and H. Kawano (1994), The GEOTAIL magnetic field experiment, *J. Geomagn. Geoelec.*, *46*, 7–21.

Lee, J. H., and V. Angelopoulos (2014), On the presence and properties of cold ions near Earth's equatorial magnetosphere, *J. Geophys. Res. Space Physics*, *119*, 1749–1770, doi:10.1002/2013JA019305.

Lennartsson, W., and E. G. Shelley (1986), Survey of 0.1- to 16-keV/e plasma sheet ion composition, *J. Geophys. Res.*, *91*(A3), 3061–3076, doi:10.1029/JA091iA03p03061.

Lin, Y., L. C. Lee, and M. Yan (1996), Generation of dynamic pressure pulses downstream of the bow shock by variations in the interplanetary magnetic field orientation, *J. Geophys. Res.*, *101*(A1), 479–493.

Lockwood, M., J. H. Waite Jr., T. E. Moore, C. R. Chappell, and M. O. Chandler (1985), The cleft ion fountain, *J. Geophys. Res.*, *90*(A10), 9736–9748.

Maggiolo, R., and L. M. Kistler (2014), Spatial variation in the plasma sheet composition: Dependence on geomagnetic and solar activity, *J. Geophys. Res. Space Physics*, *119*, 2836–2857, doi:10.1002/2013JA019517.

Matsumoto, H., I. Nagano, R. R. Anderson, H. Kojima, K. Hashimoto, M. Tsutsui, T. Okada, I. Kimura, Y. Omura, and M. Okada (1994), Plasma wave observations with GEOTAIL spacecraft, *J. Geomagn. Geoelec.*, *46*, 59–95.

Menk, F. W., and C. L. Waters (2013), *Magnetoseismology*, 251 pp., Wiley-VCH, Weinheim, Germany.

Min, K., J. Bortnik, R. E. Denton, K. Takahashi, J. Lee, and H. J. Singer (2013), Quiet time equatorial mass density distribution derived from AMPTE/CCE and GOES using the magnetoseismology technique, *J. Geophys. Res. Space Physics*, *118*, 6090–6105, doi:10.1002/jgra.50563.

Miura, A. (1984), Anomalous transport by magnetohydrodynamic Kelvin-Helmholtz instabilities in the solar wind-magnetosphere interaction, *J. Geophys. Res.*, *89*(A2), 801–818, doi:10.1029/JA089iA02p00801.

Mouikis, C. G., L. M. Kistler, Y. H. Liu, B. Klecker, A. Korth, and I. Dandouras (2010), H^+ and O^+ content of the plasma sheet at 15–19 Re as a function of geomagnetic and solar activity, *J. Geophys. Res.*, *115*, A00J16, doi:10.1029/2010JA015978.

Mukai, T., S. Machida, Y. Saito, M. Hirahara, T. Terasawa, N. Kaya, T. Obara, M. Ejiri, and A. Nishida (1994), The low energy particle (LEP) experiment onboard the GEOTAIL satellite, *J. Geomagn. Geoelec.*, *46*, 669–692.

Nosé, M., T. Iyemori, M. Sugiura, and J. A. Slavin (1995), A strong dawn/dusk asymmetry in Pc5 pulsation occurrence observed by the DE-1 satellite, *Geophys. Res. Lett.*, *22*(15), 2053–2056.

Nosé, M., A. Ieda, and S. P. Christon (2009), Geotail observations of plasma sheet ion composition over 16 years: On variations of average plasma ion mass and O^+ triggering substorm model, *J. Geophys. Res.*, *114*, A07223, doi:10.1029/2009JA014203.

Nosé, M., K. Takahashi, R. R. Anderson, and H. J. Singer (2011), Oxygen torus in the deep inner magnetosphere and its contribution to recurrent process of O^+-rich ring current formation, *J. Geophys. Res.*, *116*, A10224, doi:10.1029/2011JA016651.

Nykyri, K., and A. Otto (2001), Plasma transport at the magnetospheric boundary due to reconnection in Kelvin-Helmholtz vortices, *Geophys. Res. Lett.*, *28*(18), 3565–3568, doi:10.1029/2001GL013239.

Ohtani, S., M. Nosé, S. P. Christon, and A. T. Y. Lui (2011), Energetic O^+ and H^+ ions in the plasma sheet: Implications for the transport of ionospheric ions, *J. Geophys. Res.*, *116*, A10211, doi:10.1029/2011JA016532.

Øieroset, M., T. D. Phan, V. Angelopoulos, J. P. Eastwood, J. McFadden, D. Larson, C. W. Carlson, K.-H. Glassmeier, M. Fujimoto, and J. Raeder (2008), THEMIS multi-spacecraft observations of magnetosheath plasma penetration deep into the dayside low-latitude magnetosphere for northward and strong By IMF, *Geophys. Res. Lett.*, *35*, L17S11, doi:10.1029/2008GL033661.

Otto, A., and D. H. Fairfield (2000), Kelvin-Helmholtz instability at the magnetotail boundary: MHD simulation and comparison with Geotail observations, *J. Geophys. Res.*, *105*(A9), 21,175–21,190, doi:10.1029/1999JA000312.

Press, W. H., B. P. Flannery, S. A. Teukolsky, and W. T. Vetterling (1986), *Numerical Recipes*, Cambridge Univ. Press, New York.

Rème, H., et al. (1997), The cluster ion spectrometry experiment, *Space Sci. Rev.*, *79*(1-2), 303–350.

Roberts, W. T., Jr., J. L. Horwitz, R. H. Comfort, C. R. Chappell, J. H. Waite Jr., and J. L. Green (1987), Heavy ion density enhancements in the outer plasmasphere, *J. Geophys. Res.*, *92*(A12), 13,499–13,512.

Singer, H. J., and M. G. Kivelson (1979), The latitudinal structure of Pc5 waves in space: Magnetic and electric field observations, *J. Geophys. Res.*, *84*, 7213–7222.

Singer, H. J., D. J. Southwood, R. J. Walker, and M. G. Kivelson (1981), Alfvén wave resonances in a realistic magnetospheric magnetic field geometry, *J. Geophys. Res.*, *86*(A6), 4589–4596.

Song, P., and C. T. Russell (1992), Model of the formation of the low-latitude boundary layer for strongly northward interplanetary magnetic field, *J. Geophys. Res.*, *97*(A2), 1411–1420, doi:10.1029/91JA02377.

Southwood, D. J., and M. G. Kivelson (1990), The magnetohydrodynamic response of the magnetospheric cavity to changes in solar wind pressure, *J. Geophys. Res.*, *95*(A3), 2301–2309.

Takahashi, K., and R. E. Denton (2007), Magnetospheric seismology using multiharmonic toroidal waves observed at geosynchronous orbit, *J. Geophys. Res.*, *112*, A05204, doi:10.1029/2006JA011709.

Takahashi, K., R. E. Denton, and D. Gallagher (2002), Toroidal wave frequency at L = 6–10: Active Magnetospheric Particle Tracer Explorers/CCE observations and comparison with theoretical model, *J. Geophys. Res.*, *107*(A2), 1020, doi:10.1029/2001JA000197.

Takahashi, K., R. E. Denton, R. R. Anderson, and W. J. Hughes (2006), Mass density inferred from toroidal wave frequencies and its comparison to electron density, *J. Geophys. Res.*, *111*, A01201, doi:10.1029/2005JA011286.

Takahashi, K., R. E. Denton, S. Ohtani, W. J. Hughes, and R. R. Anderson (2008), Ion composition in the plasma trough and plasma plume derived from a Combined Release and Radiation Effects Satellite magnetoseismic study, *J. Geophys. Res.*, *113*, A12203, doi:10.1029/2008JA013248.

Takahashi, K., R. E. Denton, and H. J. Singer (2010), Solar cycle variation of geosynchronous plasma mass density derived from the frequency of standing Alfvén waves, *J. Geophys. Res.*, *115*, A07207, doi:10.1029/2009JA015243.

Terasawa, T., et al. (1997), Solar wind control of density and temperature in the near-Earth plasma sheet: WIND/GEOTAIL collaboration, *Geophys. Res. Lett.*, *24*(8), 935–938, doi:10.1029/96GL04018.

Thomsen, M. F., J. E. Borovsky, R. M. Skoug, and C. W. Smith (2003), Delivery of cold, dense plasma sheet material into the near-Earth region, *J. Geophys. Res.*, *108*(A4), 1151, doi:10.1029/2002JA009544.

Tsuruda, K., H. Hayakawa, M. Nakamura, T. Okada, A. Matsuoka, F. S. Mozer, and R. Schmidt (1994), Electric field measurements on the GEOTAIL satellite, *J. Geomagn. Geoelec.*, *46*, 693–711.

Tsyganenko, N. A., and M. I. Sitnov (2005), Modeling the dynamics of the inner magnetosphere during strong geomagnetic storms, *J. Geophys. Res.*, *110*, A03208, doi:10.1029/2004JA010798.

Ulrich, T. J., and T. N. Bishop (1975), Maximum entropy spectral analysis and autoregressive decomposition, *Rev. Geophys. Space Phys.*, *13*, 183–200.

Vellante, M., M. Förster, U. Villante, T. L. Zhang, and W. Magnes (2007), Solar activity dependence of geomagnetic field line resonance frequencies at low latitudes, *J. Geophys. Res.*, *112*, A02205, doi:10.1029/2006JA011909.

Wang, C.-P., L. R. Lyons, J. M. Weygand, T. Nagai, and R. W. McEntire (2006), Equatorial distributions of the plasma sheet ions, their electric and magnetic drifts, and magnetic fields under different interplanetary magnetic field B_z conditions, *J. Geophys. Res.*, *111*, A04215, doi:10.1029/2005JA011545.

Waters, C. L., F. W. Menk, and B. J. Fraser (1991), The resonance structure of low latitude Pc3 geomagnetic pulsations, *Geophys. Res. Lett.*, *18*(12), 2293–2296.

Williams, D. J., R. W. McEntire, C. Schlemm Ii, A. T. Y. Lui, G. Gloeckler, S. P. Christon, and F. Gliem (1994), GEOTAIL energetic particles and ion composition instrument, *J. Geomagn. Geoelec.*, *46*, 39–57.

Yau, A., and M. André (1997), Source of ion outflow in the high latitude ionosphere, *Space Sci. Rev.*, *80*, 1–25.

Yau, A. W., P. H. Beckwith, W. K. Peterson, and E. G. Shelley (1985), Long-term (solar cycle) and seasonal variations of upflowing ionospheric ion events at DE 1 altitudes, *J. Geophys. Res.*, *90*, 6395–6407.

Young, D. T., H. Balsiger, and J. Geiss (1982), Correlation of magnetospheric ion composition with geomagnetic and solar activity, *J. Geophys. Res.*, *87*(A11), 9077–9096.